



## Spatiotemporal patterns of changes in maximum and minimum temperatures in multi-model simulations

Liming Zhou,<sup>1</sup> Robert E. Dickinson,<sup>1</sup> Paul Dirmeyer,<sup>2</sup> Aiguo Dai,<sup>3</sup> and Seung-Ki Min<sup>4</sup>

Received 1 October 2008; revised 14 November 2008; accepted 4 December 2008; published 23 January 2009.

[1] This paper analyzes and attributes spatial and temporal patterns of changes in the diurnal cycle of land surface air temperature in 20 simulations from 11 global coupled atmosphere-ocean general circulation models during the 20th century and the 21st century under the SRES A1B scenario. Most of the warming in the maximum ( $T_{\max}$ ) and minimum ( $T_{\min}$ ) temperatures from 1900 to 2099 is attributed to enhanced surface downward longwave radiation (DLW), while changes in surface downward shortwave radiation (DSW) and cloud cover mainly contribute to the simulated decrease in the diurnal temperature range (DTR). Although the simulated DTR decreases are much smaller than the observed during the 20th century, the models unanimously predict substantial warming in both  $T_{\max}$  and  $T_{\min}$  and decreases in DTR, especially in high latitudes during the 21st century, in response to enhanced global-scale anthropogenic forcings (particularly greenhouse effects of atmospheric water vapor and in part aerosol radiative cooling in the tropics) and increased cloudiness in high latitudes. **Citation:** Zhou, L., R. E. Dickinson, P. Dirmeyer, A. Dai, and S.-K. Min (2009), Spatiotemporal patterns of changes in maximum and minimum temperatures in multi-model simulations, *Geophys. Res. Lett.*, *36*, L02702, doi:10.1029/2008GL036141.

### 1. Introduction

[2] The observed global-mean surface temperature has increased by about 0.74°C from 1906–2005, with the largest increase over land and larger warming rates since 1950 [Intergovernmental Panel on Climate Change (IPCC), 2007]. The minimum air temperature ( $T_{\min}$ ) has increased faster than the maximum air temperature ( $T_{\max}$ ) and thus the diurnal temperature range (DTR) has decreased over land by about 0.07°C per decade from 1950–2004, with most of the decrease occurring prior to 1980 [Vose *et al.*, 2005; Zhou *et al.*, 2008]. Associated with this asymmetric warming are changes in extremes of weather and climate, e.g., reduced frost days, increased warm nights, reduced cold nights, lengthened heat wave duration, and increased heavy precipitation [IPCC, 2007].

[3] Global coupled atmosphere-ocean general circulation models (AOGCMs) are generally able to reproduce the observed warming and the changes in temperature extremes by including effects of natural and anthropogenic forcings,

especially in the latter half of the 20th century, and such changes are found to be outside the range of natural internal variability estimated from the models [IPCC, 2007]. The models simulate a general decrease in DTR in a warmer climate, but the magnitude of the DTR decrease is much smaller than observed, due in part to the models' underestimate of increases in cloud cover [Stone and Weaver, 2003; Braganza *et al.*, 2004].

[4] Observational analyses have attributed the reduction of DTR mainly to increases of cloud cover, precipitation, and soil moisture [Karl *et al.*, 1993; Dai *et al.*, 1999]. Zhou *et al.* [2007, 2008] suggest that some of the observed DTR trends might be due to large-scale effects of increased greenhouse gases (GHGs) and aerosols. To attribute the observed DTR changes, AOGCMs are often used to separate impacts of changes in clouds versus other controlling factors. Previous studies used either simple models or one or several individual global coupled models to assess DTR changes in the 20th and/or 21st century [e.g., Stone and Weaver, 2003; Braganza *et al.*, 2004].

[5] Here we quantify changes in  $T_{\max}$ ,  $T_{\min}$ , and DTR using 20th and 21st century climate simulations from 11 global coupled AOGCMs, with most participating in the Coupled Model Intercomparison Project (CMIP3) of the World Climate Research Program (WCRP). Due to limits in the availability, spatial coverage, and accuracy of observations, especially for cloud cover, detailed validations of model simulations with observations since the 1950s will be addressed elsewhere. This study focuses on understanding and attributing spatiotemporal patterns of changes in the simulated diurnal cycle of temperature from 1900 to 2099.

### 2. Models and Simulations

[6] We analyze monthly means of daily  $T_{\max}$ ,  $T_{\min}$ , and DTR data in multi-model simulations for the 20th and 21st century, which are available at monthly or daily scales from the data portals at PCMDI (<http://www.pcmdi.llnl.gov/>), NCAR (<http://www.earthsystemgrid.org/>) and GFDL (<http://nomads.gfdl.noaa.gov/>). The 20th century simulations (20C3M) include combinations of time-evolving changes in anthropogenic (GHGs and sulfate aerosols) and/or natural (solar and volcanic) forcing agents. The 21st century simulations used here follow the SRES A1B scenario (a mid-range positive radiative forcing). In total, there are 20 simulations from 11 AOGCMs that have continuous archives of  $T_{\min}$  and  $T_{\max}$  data for 1900–2099. These models (simulations) are CCSM3 (4), CSIRO-Mk3.0 (1), CSIRO-Mk3.5 (1), GFDL-CM2.0 (1), GFDL-CM2.1 (1), ECHO-G (3), GISS-AOM (2), MIROC3.2-medres (3), MIROC3.2-hires (1), MPI-ECHAM5 (1), and PCM1 (2). Averaging over multiple members enhances the forced signal and reduces noise from

<sup>1</sup>School of Earth and Atmospheric Sciences, Georgia Institute of Technology, Atlanta, Georgia, USA.

<sup>2</sup>Center for Ocean-Land-Atmosphere Studies, Calverton, Maryland, USA.

<sup>3</sup>National Center for Atmospheric Research, Boulder, Colorado, USA.

<sup>4</sup>Climate Research Division, Environment Canada, Downsview, Ontario, Canada.

internally generated variability and errors from individual models. Here we simply average the 20 simulations to generate the multi-model ensemble mean and its standard deviation (STD). The coefficient of variation (COV), defined as the ratio of the STD to the mean (i.e.,  $\text{STD}/\text{mean}$ ), is calculated to measure inter-model (and also in part inter-ensemble), but for simplicity, we refer to it hereafter as inter-model disparity—the bigger the COV value, the larger the inter-model variability (or the less the inter-model consistency).

[7] To attribute the simulated temperature changes, we also analyzed monthly data of total cloud cover (TCC), surface downward longwave radiation (DLW), and surface downward shortwave radiation (DSW). For all variables, monthly anomalies were first computed relative to the 1900–1919 mean and were then aggregated to generate annual anomaly time series from 1900 to 2099. They were spatially remapped onto a  $5^\circ \times 5^\circ$  grid box. We calculated the global mean time series by area-weighted averaging over land, allowing for the percentage of land area per grid box. Similar averaging was performed to calculate the zonal mean time series for two broad latitudinal bands,  $50^\circ\text{S}$ – $50^\circ\text{N}$  (referred to as lower latitudes) and poleward of  $50^\circ$  in both hemispheres (referred to as subpolar), to examine the geographic contrast of TCC changes. An 11-point (i.e., 11-year) running averaging was applied in some cases to the global and zonal mean time series for analyzing low-pass filtered trends.

### 3. Results and Discussion

[8] The global mean low-pass filtered annual  $T_{\text{max}}$ ,  $T_{\text{min}}$ , and DTR anomaly time series over land for the multi-model ensemble mean and its one STD from 1900 to 2099, along with those of TCC, DSW and DLW, are shown in Figure 1 (black lines). Relative to the 1900–1919 mean,  $T_{\text{max}}$  and  $T_{\text{min}}$  increase by  $0.90 \pm 0.24^\circ\text{C}$  (i.e., the mean  $\pm 1$  STD for the filtered values, defined similarly thereafter) and  $1.04 \pm 0.27^\circ\text{C}$  in 1999, and by  $4.21 \pm 0.82^\circ\text{C}$  and  $4.51 \pm 0.78^\circ\text{C}$  in 2099, respectively. DTR consequently decreases by  $0.14 \pm 0.05^\circ\text{C}$  in 1999 and  $0.30 \pm 0.17^\circ\text{C}$  in 2099. TCC decreases slightly by  $0.15 \pm 0.35\%$  in 1999 and  $1.02 \pm 1.13\%$  in 2099. DSW decreases by  $2.64 \pm 0.81 \text{ W/m}^2$  in 1999 and  $4.59 \pm 2.35 \text{ W/m}^2$  in 2099, while DLW increases significantly by  $6.50 \pm 1.44 \text{ W/m}^2$  in 1999 and  $27.37 \pm 4.41 \text{ W/m}^2$  in 2099. The significant and persistent increase in DLW reflects mainly the greenhouse effects of a warmer and wetter atmosphere and to some extent a warmer surface. All these changes in the ensemble mean except TCC in 1999 are statistically significant ( $p < 0.05$ ) relative to the 1900–1919 mean. The changes are small prior to the 1950s and become accelerated thereafter and are much large in the 21st century. The spread of  $\pm 1$  STD with time results from differences in both forcing estimates and model physics. Based on COV values, the changes in  $T_{\text{max}}$ ,  $T_{\text{min}}$ , and DLW are most consistent among the models, followed by DSW and DTR, while TCC has the largest variation or the least consistent change signal.

[9] The zonal mean time series generally show low-pass filtered trends (red and green lines respectively in Figure 1) similar to the global mean time series. From 1900 to 2099,  $T_{\text{max}}$  and  $T_{\text{min}}$  increase more in the subpolar region than in the lower latitudes while DLW shows the opposite; DTR and DSW decrease similarly in both zones, most in the subpolar,

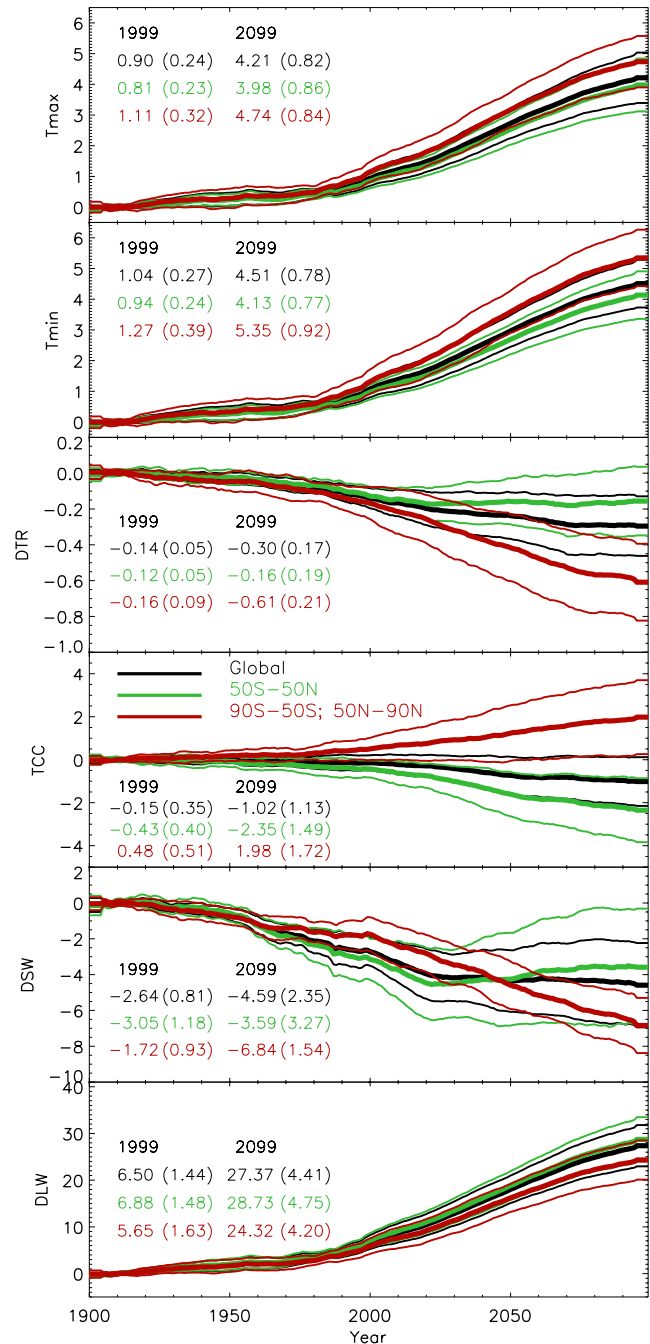


**Figure 1.** Globally (black) and zonally (red for subpolar, green for lower latitudes) averaged annual anomaly time series of  $T_{\text{max}}$  ( $^\circ\text{C}$ ),  $T_{\text{min}}$  ( $^\circ\text{C}$ ), DTR ( $^\circ\text{C}$ ), TCC (%), DSW ( $\text{W/m}^2$ ), and DLW ( $\text{W/m}^2$ ) for the multi-model ensemble mean, relative to the period 1900 to 1919, over land in the 20th and 21st century. The solid line represents the ensemble mean and the two thin solid lines denote the range of one standard deviation (STD). Values listed are the ensemble mean and one STD (in parenthesis) in 1999 and 2099. An 11-point (11-year) running averaging was applied (with the first and last five year values replaced by their five-year averages).

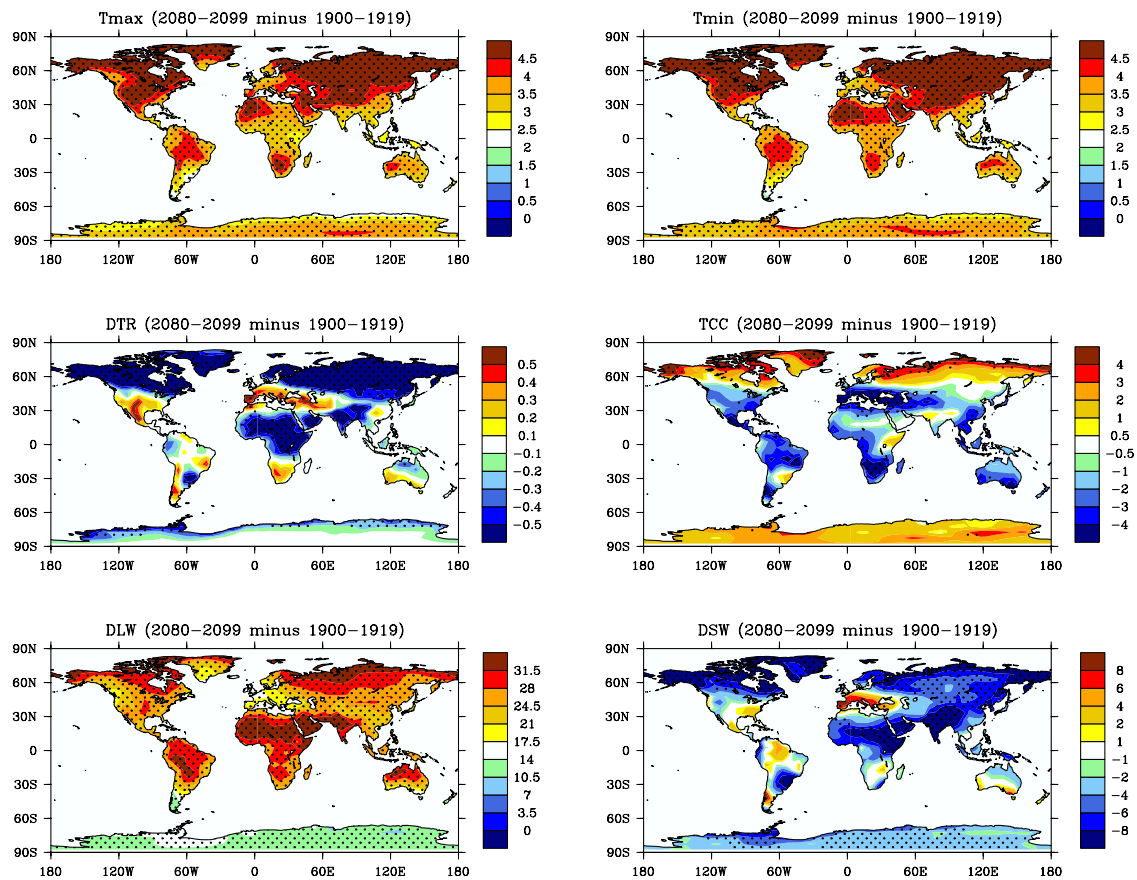


**Figure 2.** Geographical patterns of differences in the multi-model ensemble means of  $T_{\max}$  ( $^{\circ}\text{C}$ ),  $T_{\min}$  ( $^{\circ}\text{C}$ ), DTR ( $^{\circ}\text{C}$ ), TCC (%), DLW ( $\text{W}/\text{m}^2$ ), and DSW ( $\text{W}/\text{m}^2$ ), for the 2080 to 2099 mean (SRES A1B scenario) relative to the 1900 to 1919 mean (20C3M). Stippling denotes areas where the magnitude of the multi-model ensemble mean exceeds the inter-model STD (i.e.,  $|\text{COV}| < 1$ ).

and their decrease reverses slightly in the lower latitudes after 2020s; TCC increases only in the subpolar.

[10] Spatial patterns of the 2080–2099 minus 1900–1919 difference of  $T_{\max}$ ,  $T_{\min}$ , DTR, TCC, DSW, and DLW for the multi-model ensemble mean are shown in Figure 2.  $T_{\max}$  and  $T_{\min}$  rise everywhere, particularly in northern high latitudes. DTR declines over most land areas, especially in northern high latitudes, except for some increases over the Mediterranean and Middle East, USA, southern Africa, and part of South America. Interestingly, the DTR also decreases significantly over tropical Africa, the Arabian Peninsula, and southeastern Asia. Changes in DTR correspond well in the spatial pattern and magnitude to those in TCC ( $r = -0.66$ ,  $p < 0.01$ ) and DSW ( $r = 0.81$ ,  $p < 0.01$ ), respectively. A weaker but significant correlation also exists between DTR and DLW ( $r = -0.47$ ,  $p < 0.01$ ). We calculated the percentage of grid boxes with  $|\text{COV}| < 1$  (i.e., the absolute COV value less than 1) to quantify the spatial extent of inter-model consistency: 99.7% for  $T_{\max}$  and  $T_{\min}$ , 99.6% for DLW, 61.3% for DSW, 54.7% for DTR, and 31.4% for TCC. Evidently, the changes in  $T_{\max}$ ,  $T_{\min}$  and DLW are most consistent globally, while the changes in TCC differ greatly over many regions.

[11] Since TCC is very effective in changing DTR/DSW, one would expect to see a dominant negative relation between TCC and DTR/DSW, as shown in Figure 2. However, the lower latitude downward trend in both DTR and TCC

(Figure 1) and the stronger spatial correlation between DTR and DSW than that between DTR and TCC (Figure 2) suggest that non-cloud factors are also involved in decreasing the DTR. To separate the cloud versus non-cloud effects, we examined the 2080–2099 minus 1900–1919 differences in clear-sky and cloudy-sky (calculated as all-sky minus clear-sky) DSW and DLW (Figure 3). As expected, changes in cloudy-sky DSW and DLW resemble those in TCC. Changes in clear-sky DLW and DSW resemble increases in atmosphere water vapor content (figure not shown), particularly in  $30^{\circ}\text{S}–30^{\circ}\text{N}$ , suggesting the dominant effects of increasing GHGs (especially enhanced water vapor) on increasing DLW and decreasing DSW. Note that the changes in clear-sky DSW and DLW can result from those in (i) total clear-sky areas and/or (ii) clear-sky conditions (e.g., water vapor, aerosols). Our results indicate that the latter plays a major role. The positive cloudy-sky DSW anomaly (due to decreased TCC) is mostly cancelled by the negative clear-sky DSW anomaly, resulting in minor changes in the all-sky DSW and thus in the DTR, over the tropics in South and North America, and southeastern Asia. To quantify the relative contribution of TCC to DSW and DLW, we examined the global and zonal mean clear-sky versus all-sky anomalies for 1900–2099 over land (Figure 3). The all-sky versus clear-sky values show small changes ( $< 4 \text{ W}/\text{m}^2$ ) in DLW but substantial differences in DSW. The all-sky (clear-sky) DSW

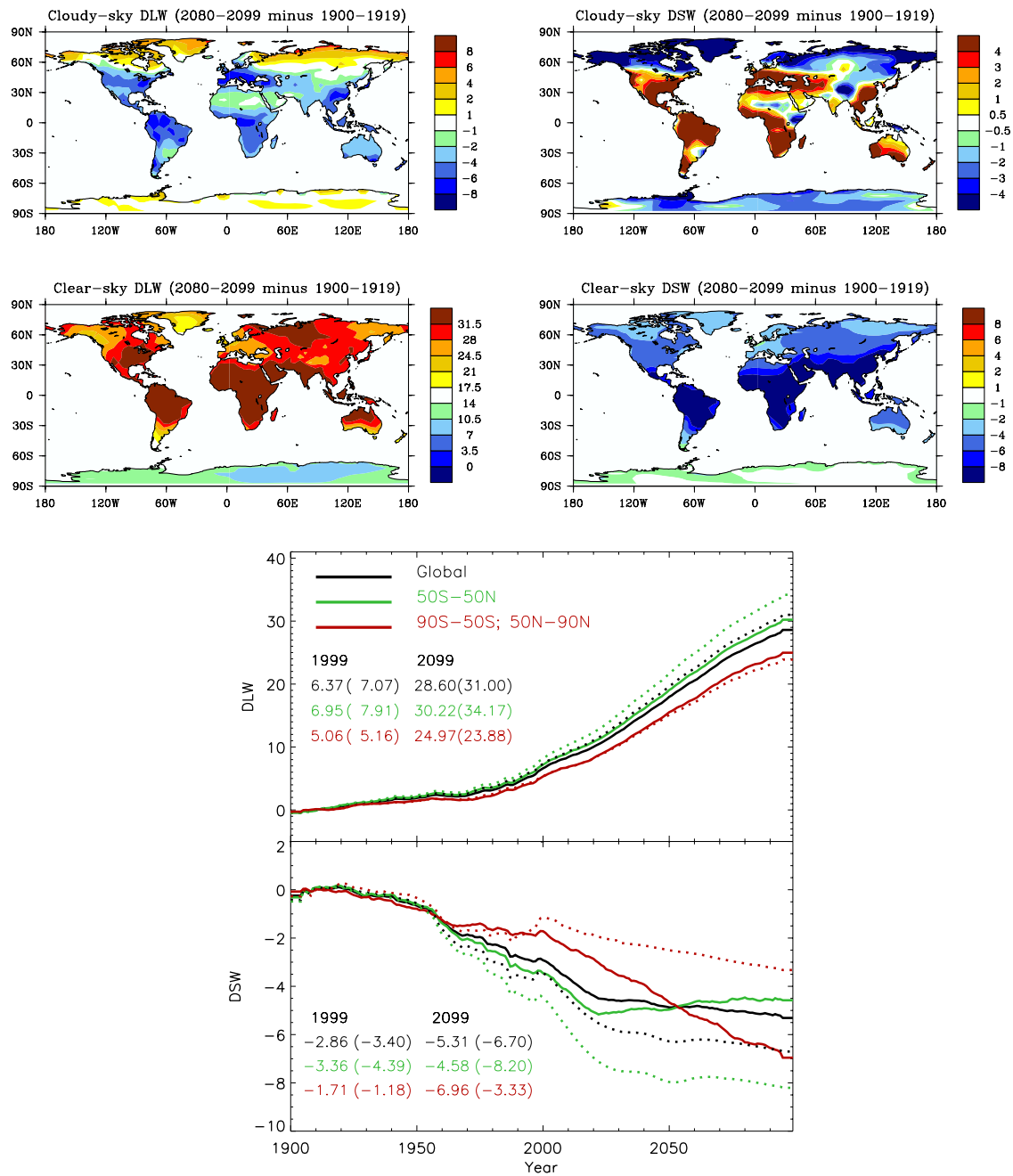


**Figure 3.** Changes in the multi-model ensemble means of cloudy-sky (or all-sky) and clear-sky DLW ( $\text{W/m}^2$ ) and DSW ( $\text{W/m}^2$ ). (top) Geographical patterns of differences in cloudy-sky and clear-sky DLW and DSW (the 2080–2099 mean minus the 1900–1919 mean). (bottom) Globally (black) and zonally (red for subpolar, green for lower latitudes) averaged annual anomaly time series of clear-sky (dashed lines) and all-sky (solid lines) DSW and DLW over land from 1900 to 2099 (values listed are the all-sky and clear-sky (in parenthesis) ensemble mean in 1999 and 2099). Note that only 14 (11) of the 20 simulations that have both all-sky and clear-sky DSW (DLW) data available are used, and an 11-point running averaging was applied to the time series as in Figure 1.

decreases by 86% (97%) from  $-2.86$  ( $-3.40$ ) in 1999 to  $-5.31$  ( $-6.70$ )  $\text{W/m}^2$  in 2099 for the global average; decreases by 36% (87%) from  $-3.36$  ( $-4.39$ ) in 1999 to  $-4.58$  ( $-8.20$ )  $\text{W/m}^2$  in 2099 for the lower latitude zonal average, and decreases by 307% (182%) from  $-1.71$  ( $-1.18$ ) in 1999 to  $-6.96$  ( $-3.33$ )  $\text{W/m}^2$  in 2099 for the subpolar zonal average. Note that the subpolar changes could also reflect seasonal changes, as the DSW (and to a lesser extent

DLW) is very small outside summer. Evidently, DSW can be substantially modified inversely by changes in TCC, especially in the subpolar zone, and also by enhanced aerosols and water vapor, especially in lower latitudes, but those factors have a small impact on DLW relative to the all-sky values.

[12] To further attribute the temperature changes, we analyze statistically changes in  $T_{\max}$ ,  $T_{\min}$ , and DTR and their association with TCC, DLW, and DSW for the multi-model

**Table 1.** Statistical Relationship Between Changes in Annual  $T_{\max}$ ,  $T_{\min}$ , and DTR, and Changes in Annual TCC, DLW, and DSW for the Period 1900–2100<sup>a</sup>

	Climate Zone <sup>b</sup>	TCC		DLW <sup>c</sup>		DSW <sup>c</sup>	
		R <sup>2</sup>	$\beta_1$	R <sup>2</sup>	$\beta_1$	R <sup>2</sup>	$\beta_1$
$T_{\max}$	GL	0.04	<b>-0.13</b>	0.73(0.77)	<b>0.16(0.16)</b>	0.08(0.09)	<b>0.16(0.13)</b>
	LL	0.03	<b>-0.08</b>	0.64(0.72)	<b>0.14(0.14)</b>	0.09(0.08)	<b>0.14(0.12)</b>
	SP	0.00	-0.02	0.73(0.74)	<b>0.20(0.22)</b>	0.04(0.08)	<b>0.10(0.13)</b>
$T_{\min}$	GL	0.01	-0.06	0.80(0.82)	<b>0.16(0.15)</b>	0.05(0.08)	<b>0.12(0.12)</b>
	LL	0.00	-0.01	0.78(0.82)	<b>0.14(0.13)</b>	0.05(0.07)	<b>0.10(0.11)</b>
	SP	0.00	0.05	0.76(0.76)	<b>0.21(0.24)</b>	0.02(0.07)	<b>0.07(0.13)</b>
DTR	GL	0.22	<b>-0.08</b>	0.00(0.00)	0.00(0.00)	0.31(0.04)	<b>0.03(0.01)</b>
	LL	0.28	<b>-0.08</b>	0.00(0.01)	0.00(0.01)	0.42(0.05)	<b>0.04(0.01)</b>
	SP	0.16	<b>-0.07</b>	0.08(0.06)	<b>-0.01(-0.01)</b>	0.16(0.01)	<b>0.03(0.01)</b>

<sup>a</sup>DLW—surface downward longwave radiation ( $\text{W/m}^2$ ), DSW—surface downward shortwave radiation ( $\text{W/m}^2$ ), TCC—total cloud cover (%). The low-pass filtered (11-year running averaging) trends were removed from the original time series.

<sup>b</sup>Climate zones: Global (GL), lower latitudes:  $50^\circ\text{S}$ – $50^\circ\text{N}$  (LL), and subpolar:  $90$ – $50^\circ\text{S}$  and  $50$ – $90^\circ\text{N}$  (SP). Regression coefficients,  $\beta_1$ , in bold are statistically significant ( $p < 0.01$ ).

<sup>c</sup>Values in parenthesis are results for clear-sky conditions.

ensemble global and zonal mean time series from 1900 to 2099 (Table 1), after removing the low-pass filtered trends (Figure 1). The regression coefficient ( $\beta_1$ ) in Table 1 represents changes in temperatures ( $T_{\max}$ ,  $T_{\min}$ , and DTR) given a unit change in TCC, DLW, and DSW. An increase in TCC or a decrease in DSW is effective in reducing DTR through a larger impact on  $T_{\max}$  than  $T_{\min}$ . Increased DLW warms  $T_{\max}$  and  $T_{\min}$  at a comparable rate and thus has a minor impact on DTR except on the subpolar region. Clear-sky and all-sky DLW shows little differences in  $\beta_1$ , suggesting minor TCC impacts on DLW, while clear-sky DSW still have some impacts on reducing DTR. Evidently, changes in DLW explain most ( $\leq 82\%$ ) of the changes in  $T_{\max}$  and  $T_{\min}$  while TCC and DSW explain most ( $\leq 28\%$  and  $\leq 42\%$ , respectively) of the DTR changes. Interestingly, DSW explains more DTR variations than TCC in the lower latitudes.

[13] The model simulated DTR decreases over most areas of  $50^\circ\text{S}$ – $50^\circ\text{N}$  are likely a result of effects of GHGs and in part increasing aerosols. Should the decreased TCC be mainly responsible for the DTR changes over the areas, one would see an increase of DTR, rather than the modeled widespread decrease. The large decrease in DTR in northern high latitudes mainly reflects the effects of increased TCC. Increasing GHGs in a warmer and wetter climate (especially enhanced atmosphere water vapor content) can significantly increase DLW and increasing atmospheric water vapor as a solar absorber can also reduce DSW, especially in the tropics, as shown in Figure 3. Increasing aerosols cool the surface at daytime through reduced solar heating (i.e., DSW), which cause less daytime soil heat storage and thus less nighttime soil heating, i.e., a decline in DTR due to a much larger cooling in daytime than nighttime.

[14] Compared to limited observations since 1950 [Vose *et al.*, 2005; Zhou *et al.*, 2008], the magnitude of the simulated DTR decrease in the 20th century is much smaller, as previously reported [Stone and Weaver, 2003; Braganza *et al.*, 2004]. Several factors might result in the smaller simulated DTR changes. Some differences are expected, for example, because (1) observed versus simulated differ in both forcings and boundary conditions, and the models have structural and parametric uncertainties, and (2) the ensemble averaging process filters out much of the natural internal interannual variability that exists in observed time

series and is simulated by the models [IPCC, 2007]. However, we suspect that three other factors may play a major role. First, the observed increase in cloud cover is not seen in the models over most boxes. The simulated TCC shows a small decreasing trend while the observed shows the opposite over many areas [Dai *et al.*, 1999]. Although many models may still have only cover as a description of clouds, in reality clouds are more complicated than modeled and a change in drop size distribution can have a large effect. The response of clouds and their properties (e.g., optical thickness) to increasing GHGs currently represents the largest uncertainty in model predictions of cloud feedback and climate sensitivity [IPCC, 2007]. Second, the models may not represent realistically the asymmetric response of  $T_{\max}$  and  $T_{\min}$  (thus DTR) to the enhanced DLW and thus underestimate the DTR decrease. For a given forcing, temperatures are most sensitive to changes in radiative forcings under cold stable conditions with weak winds, and consequently nighttime and high-latitude temperatures (hence DTR) are strongly correlated with DLW [e.g., Betts, 2006; IPCC, 2007]. The weaker diurnal cycle of the simulated temperature than observations [IPCC, 2007] and the comparable warming effect of DLW on  $T_{\max}$  and  $T_{\min}$  indicate that the models may not realistically characterize the diurnal response of DTR to the strong and persistent DLW forcing, especially in the 21st century. Third, current AOGCMs differ largely in their inclusion of aerosol forcings, and most models only consider direct effects of limited aerosols (e.g., sulfate) but ignore aerosol indirect effects (e.g., aerosol-cloud interactions) and other types of aerosols (e.g., black carbon) that may help decrease DTR over some regions. The strong DTR-DSW correlation shown above is consistent with an observational analysis [Wild *et al.*, 2007]. Absorbing aerosols like black carbon in tropics and mid-latitudes can strongly reduce surface solar heating and thus may largely decrease regional DTR (e.g., in Southeast Asia). Most other aerosols can also affect DTR directly by reducing DSW. Larger indirect effects are expected for aerosols through their modification of cloud properties [Huang *et al.*, 2006].

#### 4. Concluding Remarks

[15] This paper analyzes spatiotemporal patterns of changes in  $T_{\max}$ ,  $T_{\min}$  and DTR from 20 multi-model

simulations in the 20th and 21st century. Our results indicate that the strong and persistent increase in DLW, which mainly reflects the greenhouse effect of a warmer and wetter atmosphere and to some extent of a warmer surface, is the dominant global forcing in explaining the simulated warming of  $T_{\max}$  and  $T_{\min}$  in the 20th and 21st century, while its effect on DTR is very small except in northern high latitudes. Changes in DSW are one order of magnitude smaller than those in DLW and thus have a small impact in the warming of  $T_{\max}$  and  $T_{\min}$ , but, together with changes in TCC, contribute most to the simulated changes in DTR. Although the magnitude of the simulated DTR decrease is much smaller than the observed during the 20th century, the models are unanimous in their prediction of substantial warming in both  $T_{\max}$  and  $T_{\min}$  and the reduction of DTR, especially in high latitudes during the 21st century, in response to enhanced global-scale anthropogenic forcings (particularly greenhouse effects of atmospheric water vapor and in part aerosol radiative cooling in the tropics) and increased cloudiness in high latitudes. The small DTR changes seen in the models during the 20th century may be mainly attributed to the lack of an increasing trend in cloud cover, deficiencies in representing the asymmetric response of  $T_{\min}$  and  $T_{\max}$  to the enhanced DLW, and the lack of some important processes that describe changes in clouds and aerosols (and their properties) in the models.

[16] **Acknowledgments.** This study was supported by the NSF grant ATM-0720619 and the DOE grant DE-FG02-01ER63198. We acknowledge PCMDI, NCAR and GFDL for collecting and archiving the model data. The National Center for Atmospheric Research is sponsored by the National Science Foundation.

## References

- Betts, A. K. (2006), Radiative scaling of the nocturnal boundary layer and the diurnal temperature range, *J. Geophys. Res.*, *111*, D07105, doi:10.1029/2005JD006560.
- Braganza, K., D. J. Karoly, and J. M. Arblaster (2004), Diurnal temperature range as an index of global climate change during the twentieth century, *Geophys. Res. Lett.*, *31*, L13217, doi:10.1029/2004GL019998.
- Dai, A., K. E. Trenberth, and T. R. Karl (1999), Effects of clouds, soil moisture, precipitation, and water vapor on diurnal temperature range, *J. Clim.*, *12*, 2451–2473.
- Huang, Y., R. E. Dickinson, and W. L. Chameides (2006), Impact of aerosol indirect effect on surface temperature over east Asia, *Proc. Natl. Acad. Sci. U. S. A.*, *103*, 4371–4376, doi:10.1073/pnas.0504428103.
- Intergovernmental Panel on Climate Change (IPCC) (2007), *Climate Change 2007: The Physical Science Basis. Contribution of Working Group I to the Fourth Assessment Report of the Intergovernmental Panel on Climate Change*, edited by S. Solomon et al., Cambridge Univ. Press, Cambridge, U. K.
- Karl, T., et al. (1993), A new perspective on recent global warming: Asymmetric trends of daily maximum and minimum temperature, *Bull. Am. Meteorol. Soc.*, *74*, 1007–1023.
- Stone, D. A., and A. J. Weaver (2003), Factors contributing to diurnal temperature range trends in twentieth and twenty-first century simulations of the CCCma coupled model, *Clim. Dyn.*, *20*, 435–445.
- Vose, R. S., D. R. Easterling, and B. Gleason (2005), Maximum and minimum temperature trends for the globe: An update through 2004, *Geophys. Res. Lett.*, *32*, L23822, doi:10.1029/2005GL024379.
- Wild, M., A. Ohmura, and K. Makowski (2007), Impact of global dimming and brightening on global warming, *Geophys. Res. Lett.*, *34*, L04702, doi:10.1029/2006GL028031.
- Zhou, L., A. Dai, Y. Dai, R. S. Vose, C.-Z. Zou, Y. Tian, and H. Chen (2008), Spatial patterns of diurnal temperature range trends on precipitation from 1950 to 2004, *Clim. Dyn.*, doi:10.1007/s00382-008-0387-5.
- Zhou, L., R. E. Dickinson, Y. Tian, R. S. Vose, and Y. Dai (2007), Impact of vegetation removal and soil aridation on diurnal temperature range in a semiarid region: Application to the Sahel, *Proc. Natl. Acad. Sci. U. S. A.*, *104*, 17,937–17,942.
- A. Dai, National Center for Atmospheric Research, 1850 Table Mesa Drive, Boulder, CO 80305, USA.
- R. Dickinson and L. Zhou, School of Earth and Atmospheric Sciences, Georgia Institute of Technology, 311 Ferst Drive, Atlanta, GA 30332, USA. (lmzhou@eas.gatech.edu)
- P. Dirmeyer, Center for Ocean-Land-Atmosphere Studies, 4041 Powder Mill Road, Suite 302, Calverton, MD 20705, USA.
- S.-K. Min, Climate Research Division, Environment Canada, 4905 Dufferin Street, Downsview, ON M3H 5T4, Canada.